ACS APPLIED MATERIALS & INTERFACES

Research Article

www.acsami.org

Composite Sensor Particles for Tuned SERS Sensing: Microfluidic Synthesis, Properties and Applications

Nikunjkumar Visaveliya,* Steffen Lenke, and J. Michael Köhler

Department of Physical Chemistry and Microreaction Technology, Technical University of Ilmenau, Weimarer Strasse 32, D-98693 Ilmenau, Germany

Supporting Information

ABSTRACT: Surface-enhanced Raman scattering (SERS) is a promising platform for particle-based sensor signaling, and droplet-based microfluidic systems are particularly advantageous for control of the size and composition of micro- and nanoparticles. For controlled sensing application, a high homogeneity of the sensor particles is a key requirement, and the particles with functional properties demand for the preparation in a minimum number of synthesis steps. Frequently used coflow and flow focusing arrangements, however, produce the microparticles of only larger size. To address such concern for downscaling of particle size, which is crucial for strong sensing outcome, we have used a peculiar micro cross-flow arrangement here for generating the polymer microparticles of broad size range between 30 and 600 μm along with in situ embedded silver nanoparticles. Embedded silver acts as nuclei for additional silver enforcement via silver-catalyzed silver deposition in order to realize the composite microparticles for SERS sensing. The homogeneous size and spatial distribution of silver nanoparticles inside the matrix and enforcement over the surface together with controlled pore size provides a high and homogeneous loading of polymer composite sensor. Moreover, different parameters such as analytes concentration and particles size have been studied here for SERS sensing application of biochemical molecules (amino acids and vitamins). Overall, the platform for size-tuned droplets generation, synthesis of composite microparticles, mechanism for synchronized photopolymerization−photoreduction, tuned silver enforcement, and the impacts of different analytes on differently composed microparticles are systematically investigated in this paper.

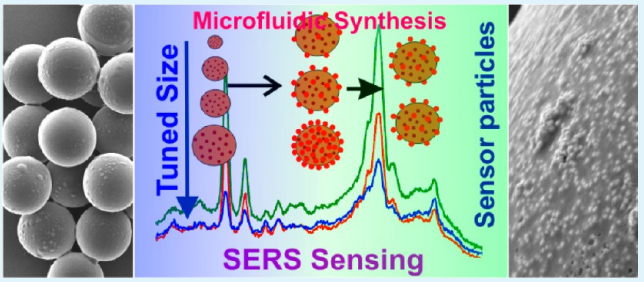

KEYWORDS: *composite microparticles, size-tuning, SERS sensing, microfluidic, droplet formation, photopolymerization and photoreduction, nanoparticles nucleation*

1. INTRODUCTION

Metal/polymer composite materials are of interest for a large spectrum of applications because they unifying the complementary properties of both classes of materials.[1,2] It includes chemical, mechanical, and electrical properties together with swellability and heat conductivity.[3,4] Both components can be varied to a large extent: metal by formation of alloys and different solid morphologies,[5,6] and polymer by the monomer types and composition in case of copolymers.[7] Composite material can be generated in the form of bulk material or in a particulate form. Microfluidic techniques[8] are particular interesting because they allow generating polymer particles or even composite particles with extraordinary high homogeneity.[9,10] The microfluidic process accomplishes a regular droplet formation resulting in a narrow size distribution of obtained microparticles. To generate the droplets of precise size is crucial in microfluidic field.[11] A single droplet contains all reactants in the picoliter or nanoliter volume,[12] and therefore their manipulation and stability is a crucial task.[13] The droplet compartmentalization, homogeneity, material synthesis and composition of heterogeneous materials are influenced by the device design.[11] A tuning of the droplet (particle) diameter can be achieved by variation in the viscosities of used liquids, by types of polymer, by size of a nozzle for releasing monomer droplets in the micro device, by wetting behavior or even simply by tuning the flow rates ratios of monomer and embedding carrier liquids.[14] In addition, this strategy, therefore, can be applicable for the generation of core/shell[15] and composite particles too.[16]

The incorporation of metal nanoparticles inside the polymer matrix is attractive for generating new types of labeling and sensing particles.[17−19] In particular, silver nanoparticle-doped gel-like polymer microparticles are of interest for the application in bead-based sensing by using surface-enhanced Raman scattering effect (SERS sensing). Co-flow[20] and flow-focusing[21,22] arrangements have been previously used for the synthesis of monodispersed polymer particles.[23,24] However, the size ranges of the particles were always in the higher

Received: January 20, 2015
Accepted: May 5, 2015
Published: May 5, 2015

DOI: 10.1021/acsami.5b00604
ACS Appl. Mater. Interfaces 2015, 7, 10742−10754

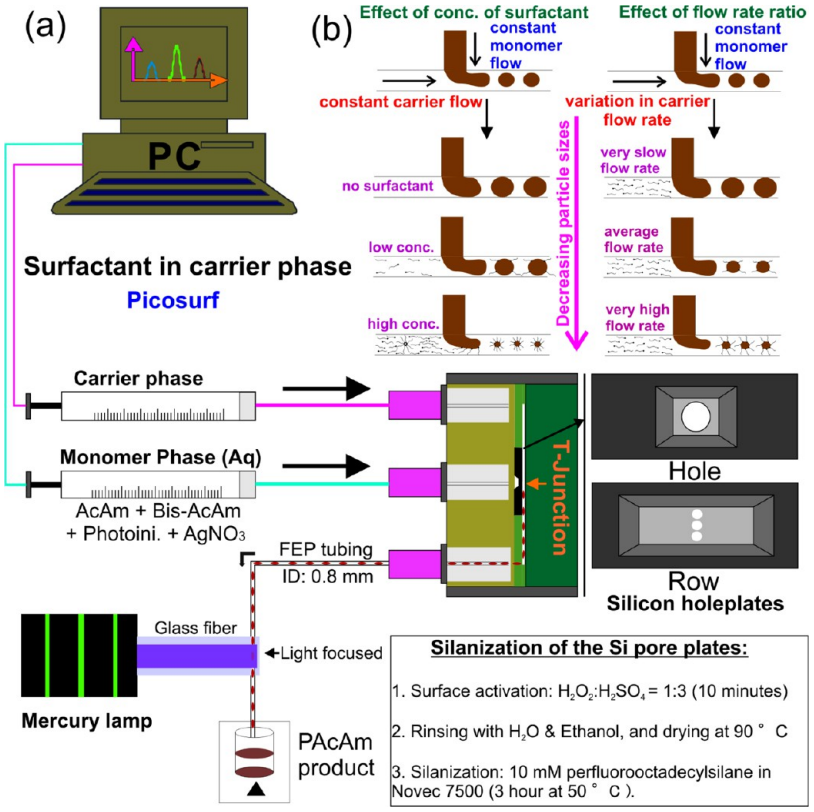

Figure 1. Schematic of (a) microfluidic arrangement for the microparticles synthesis and (b) droplet tuning mechanism in microreactor at different reaction conditions.

micrometer to submillimeter and millimeter range. To enhance the SERS signal for sensing purpose, particles should be of deeper micrometer size. Such a large reduction of particles size in flow capillary and coflow arrangement is difficult to achieve. Therefore, to address this need, we have used a distinct micro holeplate-based cross-flow microfluidic arrangement here to produce the homogeneous particles of broad size range between 30 and 600 μm.

By using lithographically designed microreactor, we successfully achieved many challenges here. The broad size range spectrum of the particles with homogeneous size distribution is a challenge. Only homogeneous particles make an impact on their application to the targeted drug delivery,[25−27] microtoxicological screening,[28] and fluorescent- and plasmonic sensing.[29] Here, by functionalizing the microchip and using a specific interfacial stabilizing agent (picosurf), we have successfully addressed those challenges for particles monodispersity and tuning of particles size in a wide range between 30 and 600 μm. Beside the size, the control of the permeability of the polymer matrix is a very important task (controlled porous size, matrix affinity, and permeability play a major role in the sensing application). In this work, suited particles have been obtained successfully by find out the critical reaction conditions. The smaller the metal nanoparticles, the higher the surface energy,[30] and therefore, to minimize the interfacial energy, smaller nanoparticles quickly aggregated.[31] To incorporate them into polymer microparticles with precise distribution (without random aggregation) for controlled sensing, a critical in situ approach, we performed here the simultaneous photopolymerization and photoreduction in a single-step synthesis in a presented microfluidic platform. The effect of increasing the silver amount reflects how a systematic tuning of the SERS signal intensity realized after controlled interaction with different analytes molecules. The sensing effects rely on the homogeneous size and well-defined surface properties of the sensor particles. Therefore, we have focused more on the qualitative synthesis of sensor particles as versatile SERS substrate in a defined microfluidic platform. Many reports for the synthesis of microparticles in the microfluidic arrangement have been published in the past several years.[32−35] However, the controlled tuning of the size and composition from deeper micrometer to submillimeter range with high homogeneity, and their application for tuned SERS sensing is not reported with full protocol. Here, we present the full coverage from synthesis to application of the sensor particles for controlled SERS sensing.

2. EXPERIMENTAL SECTION

2.1. Process Concept. Fabrication of device, generation, and manipulation of droplets as well as microgel particles, controlled distribution of silver (Ag) nanoparticles inside and over the surface, and their characterization by SERS, UV/vis, light microscopy and SEM are described here. The control over the droplet size was attained by the application of different concentrations of surfactant (fluorinated picosurf) and by applying suitable flow rate ratio of continuous and dispersed phase. The photochemical activation is responsible for a fast and homogeneous initiation during the solidification process of microfluidically formed droplets. At the same time, the reduction of Ag^+ ions to metallic Ag and the formation of Ag nanoparticles embedded in the developing polymer matrixes are initiated by a photochemical activation. The formed polymer particles are swellable in water and allow the diffusion of further water-soluble reactants inside the matrix. Therefore, Ag nanoparticles inside the polymer matrix can acts as nuclei in a second process phase for further metal-catalyzed Ag deposition. The whole process consists of the following

DOI: 10.1021/acsami.5b00604
ACS Appl. Mater. Interfaces 2015, 7, 10742−10754

steps. (A) Polymer particles formation (micro continuous-flow process): (i) Formation of monomer droplets in microreactor by shear force of the continuous phase. (ii) Transport of the droplets from the holeplate-based microreactor to the irradiation zone. (iii) Photochemical initiation promotes polymerization of monomers as well as photoreduction of Ag salt, simultaneously. (iv) Completion of polymerization process which forms in situ Ag embedded polymer microgel particles. (B) Ag enforcement (batch process): (v) Mixing the suspension of primarily formed polymer particles with depositing solution. (vi) Metal-catalyzed Ag deposition by chemical reduction of Ag^+ ions. (vii) Washing process in order to remove the unreacted impurities. (viii) Applying different concentration of analytes over the surface of composite particles for SERS measurement. (ix) The quality of sensor particles formation was characterized by SERS, UV/vis, light microscopy, and SEM.

2.2. Microreactor Fabrication. The silicon (Si) hole-plate (Figure S3 in the Supporting Information) based microreactor was prepared by a microlithographical process. To prepare this, we applied a photolithographic procedure using an optical mask aligner and a dry etching process for the micropatterning of the mask layer. The Si-chip has been placed inside a two-walled chamber. The front side of the Si chip placed in a manner where continuous phase was flowing over it. The width of the capillary slit of about 0.2 mm was adjusted between two surfaces of channel walls (Figure S2 in the Supporting Information). Monomer droplets generates at T-junction by a flowing continuous phase in dripping mode manner. The Si-membrane (0.7×0.7 mm^2) with a single hole was placed on a rectangular-shaped chamber with sloped side walls inside the Si-chip with an outer size of 0.9×0.9 mm^2.

2.3. Silanization of Si Holeplate. A Si micro holeplate chip of 40 μm hole diameter has been poured inside the H_2O_2:H_2SO_4 (1:3) solution for about 10 min for the purpose of surface activation. With this step, the surface of a chip becomes more hydrophilic with excessive hydroxyl functional groups. The Si chip then rinsed with double distilled water and successively with ethanol several times. The Si chip has been placed, afterward, inside a heating oven at 90 °C for drying. In the next step, one droplet (10 μL) of Novec 7500 and then 20 μL of perfluorooctadecylsilane were applied on the chip surface. The silanization reaction kept running for about 6 h at 50 °C. Finally, the chip was rinsed with Novec 7500 and placed inside the microreactor chamber for droplet generation at T-junction in a cross-flow microfluidic arrangement as shown in Figure 1.

2.4. Microfluidic Synthesis of Size and Composition Tuned Ag-Embedding Polyacrylamide Composite Particles. Figure 1 represents the microfluidic setup where carrier phase is a fluorinated liquid (Novec 7500) and dispersed phase is an aqueous monomer solution. Carrie phase made up of the fluorinated surfactant "picosurf" dissolved in the Novec 7500 (300 μL of 5% picosurf (in Novec 7500) in 10 mL Novec 7500). A carrier solution then filled in a 10 mL glass syringe and fixed to the syringe pump. The aqueous monomer (dispersed phases) is one component in the mixture of silver salt, monomer, cross-linker and photoinitiator. A mixture of 0.6 g of acrylamide and bis-acrylamide (19:1) was dissolved in 2 mL of deionized water. 3.8 mg silver nitrate ($AgNO_3$) was added to the above solution of acrylamide monomer. Sixteen microliter of 2-hydroxy-2-methylpropiophenone (HMPP) (photoinitiator) in 24 μL of ethylene glycol was added sequentially to the monomer solution for initiation of photopolymerization as well as photoreduction simultaneously. Both syringes were connected with lithographically prepared microreactor with two successive orifices for entries. A silanized Si chip placed inside the microreactor chamber (hole diameter is 40 μm). The UV source has been applied at an output end of micronozzle which carrying the droplet-embedding continuous flow. Droplets of the monomer phase were generated by continuous phase at T-junction of a microreactor, and polymerized subsequently in the flow to form particles at UV irradiation zone. Residence time of the droplets under UV ray in photochemical reaction station is about 0.5 s. By varying the flow rates of both antagonistic phases appropriately, the size of polyacrylamide microgel particles can be tuned in a same setup. Once the particles were formed, the carrier solution was decanted from the collection tube. Then, particles were repeatedly washed by ethanol and by deionized water several times to remove the impurities. The color of particles was yellow due to in situ formation of Ag nanoparticles inside the microgel particles during photopolymerization. Further Ag enforcement was applied on the surface of Ag embedded polyacrylamide microgel particles in a following step.

2.5. Procedure for Ag Enforcements. In the first step, Ag nanoparticles were already distributed inside the polymer matrix during in situ simultaneous photopolymerization and photoreduction process. Such embedded Ag nanoparticles initiates the further formation of Ag nanoparticles at the surface of microgel particles (through pores) via Ag-catalyzed Ag nanoparticles synthesis upon addition of Ag precursor. Therefore, to process the reaction, 50 μL of 5 mM ascorbic acid solution have been added to the microgel suspension (also further experiments with different concentrations of ascorbic acid). In subsequent step, 50 μL of 10 mM $AgNO_3$ solution were added. Immediately, the color of the matrix turns to brown or black. It indicates the formation of larger Ag nanoparticles on the surface of microgel particles. Different concentrations of $AgNO_3$ were applied for tuning the density of Ag nanoparticles on the microgel particles uniformly. Finally, the composites particles were repeatedly washed several times with deionized water and stored them at 2 °C. Ag enforcement was visualized by SEM measurements and under the light microscope. In further experiments, different analytes were applied to the composite particles for SERS measurements.

2.6. Characterization. *2.6.1. Scanning Electron Microscopy.* The scanning electron microscope (SEM) images of the polymer microparticles and composite particles were taken from the JEOL JSM 6380 instrument. For the SEM sample preparation, particles have been applied on the conductive SEM film. To cover the surface of polymer particles by a conductive layer in order to protect them by electron beam in the SEM vacuum chamber, a gold–palladium sputtering has been applied for 1 min.

2.6.2. Light Microscope Imaging. A fluorescence microscope Axioplan 2 imaging (Zeiss) with photo camera (SONY, model number: SLT-A37) was used for recording optical images of polyacrylamide composite microparticles. Ag enforced microfluidically prepared polyacrylamide microparticles have been applied on a glass slide, and brought under the light focus of a microscope.

2.6.3. Surface-Enhanced Raman Scattering (SERS) Measurement. Different densities of Ag nanoparticles were applied for characterizing the SERS effect after addition of different concentrations of analytes. A single particle or a couple of particles were filled in the small glass vial of the Raman instrument (Raman System, R-3000) for surface-enhanced Raman scattering measurement. Different intensity with optimal enhancement of the Raman light was observed after scattering due to SERS sensing. SERS signal intensities consistently increase with Ag amount and also with analyte concentrations. The laser spot size on the sample was usually 2–3 mm in diameter. Green laser with 532 nm excitation laser source and 50 mW laser power has been applied for SERS measurement of all different kinds of the sensor particles upon the application of different analytes with concentration from 10 mM down to 1 μM.

2.6.4. UV–Visible Spectroscopy. Plasmonic spectra of the sensor particles with embedded Ag and enforced Ag nanoparticles were obtained from the Specord 200 (Analytic Jena) UV/vis spectrophotometer. The particles suspension was filled in the transparent UV cuvette, and recorded the spectra at high speed (50 nm per 2 s).

3. RESULTS AND DISCUSSIONS

3.1. Droplet Generation Mechanism in the Microfluidic Arrangement. Here, a droplet-based microfluidic technique[36,37] produces the size-tuned polyacrylamide composite microgel particles. Initially, when the monomer phase enters the stream of continuous flow, the monomer liquid thread breaks-off by strong shear force of continuous liquid in a dripping mode manner to release the droplets at a T-junction in the microfluidic cross-flow arrangement (Figure 1a). The

DOI: 10.1021/acsami.5b00604
ACS Appl. Mater. Interfaces 2015, 7, 10742–10754

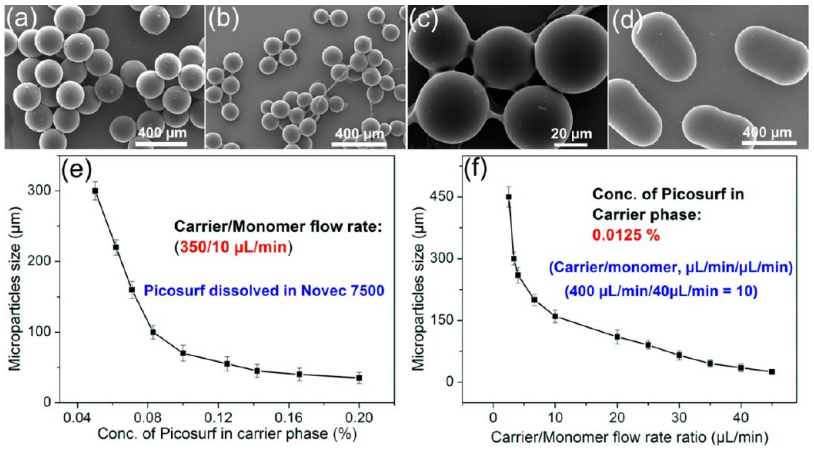

Figure 2. SEM images of the size-tuned polyacrylamide microparticles obtained in the microfluidic platform at different flow rate ratios of carrier (0.125% Picosurf in Novec 7500) and monomer phase: (a) 300/50 (carrier/monomer, μL/min), (b) 300/20, (c) 400/12 (smaller particles), and (d) 200/80 (without Picosurf in carrier phase, slug polymerized). (e, f) are the graphical representation for the effect of flow rate ratio of both immiscible liquids and concentration of surfactant on the particle sizes, respectively.

interfacial stress, therefore, is generated at droplet surface where both immiscible phases interact in the microchannel. Parameters such as surface tension due to strong shear force, viscosity of continuous phase, as well as channel diameter playing crucial role for droplet-releasing mechanism. Although there is strong impact of such parameters, the dominating consequences for the broad tuning of droplets size are governed by the addition and variation of the concentrations of picosurf in a carrier phase. The size of droplets is on the micrometer scale, and therefore the parameters such as viscosity, inertial stress, surface tension, and diffusion become more important, and can be explained in terms of the Capillary, Peclet and Reynolds numbers.[38] Surfactant decreases the surface tension of droplets and allows generating the droplets of homogeneous size by continuous breaking off the monomer thread at discrete time interval (very short). Capillary number is the ratio of viscous force to surface tension, and it defined as $Ca = \upsilon_c\mu/\gamma$, where μ is the viscosity of the fluid, υ_c is the velocity of the flow and γ is an interfacial tension.[39] The higher the picosurf concentration, the lower the surface tension at interface,[40,41] and therefore, the generated droplets are of smaller size due to higher Ca. Together with concentration of picosurf, a carrier flow rate and their viscosity impacts significantly to obtain the droplets of different size. Hence, at a higher viscosity of carrier phase, the droplets produced are of a smaller size becaues of higher *Ca* again. Similarly, strong carrier flow breaks the monomer thread early and generates droplets of smaller sizes too (high *Ca*). In a further process, the flow and the shear force depend on the channel diameter of microreactor. With identical diameter of microchannel, shear force increased with velocity of the continuous phase. Therefore, the formation of the smaller-sized droplet is led by high shear force due to higher *Ca*.[33] Viscosity of the carrier phase increases with addition of surfactant. Viscosity is the tendency for the fluid to move in parallel layers in the tube known as laminar flow. The Reynolds number is termed as the ratio of counter laminar flow force to viscous force, and is calculated as $Re = av/\nu$, where a is the surface area of channel, and v and ν are the velocity and viscosity of the applied liquid. When the shear force of a continuous flow is very high, the smaller-sized droplets of monomer phase are generated because of the high Reynolds number. A diffusion of the liquid in channel represents the Peclet number by $Pe = U_aH/D$, where U_a is the average velocity of a liquid flow, H is a characteristic length scale of the system perpendicular to the flow direction, and D is the diffusion coefficient of molecules present in the liquid. Thus, the large spectrum of droplets size can be uniformly obtained by varying the reaction parameters in the microfluidic system (Figure 1b). In contrast to the emulsion polymerization where two immiscible phases are emulsified through surfactant as a mediator, here the droplets are suspended into the carrier liquid and therefore the polymerization is a suspension photopolymerization.

3.2. Size-Tuning of Composite Microparticles. Simultaneous co-initiation of photopolymerization and Ag photoreduction during the light exposition generates the composite particles in a single step. Monodispersed droplets generation is crucial for homogeneous polymer particles production.[42,43] The stable spherical droplets of aqueous monomer phase are generated in the flowing continuous phase because the surface of Si chip modified to be fluoro-compatible. The nozzle diameter is of 500 μm, and the diameter of formed droplets is about 60 μm, which explains the fact that the droplets are embedded inside the carrier solution. Photochemical micro continuous-flow synthesis of polyacrylamide/silver composite particles initiated through fluid actuation and an exposition of the monomer droplets realized at UV irradiation zone. The color of the obtained microparticles corresponds well with typical plasmonic absorption of spherical Ag nanoparticles,[44,45] which indicates the in situ formation of Ag nanoparticles inside the matrix. When 10 mM $AgNO_3$ solution of 30% acrylamide was used, the color of the obtained composite polymer particles was bright yellow. Pale yellow, dark yellow, brown, and black colored polyacrylamide particles sequentially generated when $AgNO_3$ concentration was gradually increased (from 15 mM up to 100 mM). The catalytic property[46] of composite particles largely rely on the precise and uniform distribution of Ag nanoparticles inside the polymer matrix. As applied here, an in situ synthesis of Ag nanoparticles (photoreduction) inside the cross-linked polymer matrix is the versatile strategy to obtain the polymer−metal composite microparticles in a single-step process, which also prevent the undesired and random aggregation of smaller metal nanoparticles in the matrix interior.

DOI: 10.1021/acsami.5b00604
ACS Appl. Mater. Interfaces 2015, 7, 10742−10754

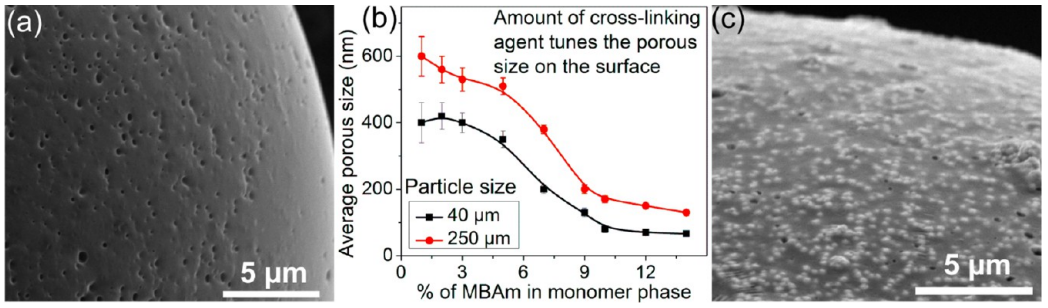

Figure 3. (a) SEM image of Ag nanoparticles embedded (60 mM) polyacrylamide particle possess porosity on the surface, (b) graphical representation for the relation between obtained porous size on polymer particles surface and cross-linking agent amount in a monomer phase, and (c) SEM image of Ag embedded (60 mM) Ag enforced (10 mM) polyacrylamide composite microparticles.

The production of droplets using a cross-flow principle should obviously occur with high reproducibility,[47] which is resulting into the high homogeneity of particles after polymerization and drying (Figure 2). The whole process is robust against a variation of flow rates of individual as well as both regimes. When 0.125% picosurf (in Novec 7500) has been used as a continuous phase, particles of about 55 μm were produced at a flow rate ratio of 35 (350:10 μL/min, carrier:monomer). The particles size consistently increases with gradual decreasing in concentration of picosurf surfactant. Therefore, particles of about 220 μm diameter were obtained when 0.062% picosurf was used again at similar flow rate ratio (35) of both immiscible phases. A late release of droplets resulted when surfactant concentration was not high enough. While there is no surfactant present in the continuous phase, the droplet release process was assisted only by the shear force of the carrier flow which depends on the viscosity and velocity of continuous phase. Without surfactant, at a flow rate ratio of 20 (200:10 μL/min, carrier/monomer), particles of about 500 μm were formed (similar to channel diameter) despite the hole diameter of Si chip was only 40 μm. Here, because of the immiscibility of dispersed phase with continuous phase, a long liquid thread is formed and finally it breaks down at longer extent. Further increase in the monomer flow with decreased carrier flow (200:80, carrier:monomer), polymer rods of about 500 μm diameter are obtained (Figure 2d). When surfactant was not present, smaller-sized particles of about 230 μm were also formed at a very high carrier flow rate (1000 μL/min). In such cases, the residence time for the generated droplets at irradiation zone is much less and hence the obtained particles are semipolymerized, which finally fused with each other in the collection tube.

The competition between flow rate ratio and concentration of surfactant to control the particles size derives from the competition between shear force and interfacial tension, and is directly related to the capillary number (Ca). At 0.062% picosurf concentration, the obtained particles are of 220 μm when flow rate ratio was 35 (350:10 μL/min, carrier:monomer). The similar-sized (about 220 μm) particles were obtained at the flow rate ratio of only 5 (200:40 μL/min, carrier:monomer) when a higher concentration of picosurf (0.125%) was used. During the competition between concentration of surfactant and shear force of continuous phase, the effect of concentration is dominating. At lower concentration of surfactant, the higher flow rate of continuous phase is responsible for a controlled and early release of the monomer droplets. In case of higher surfactant, smaller particles were formed even at lower carrier flow rate (due to surface tension minimization). Figure 2e, f summarizes the results of tuned particle size depending on the surfactant concentrations and variation in the flow rate ratios. The size tuning effect at different flow rate ratio and at different concentrations of picosurf in the carrier phase is presented in Figures S5 and S6 and Tables S1 and S2 in the Supporting Information.

3.3. Ag-Enforcement for Enhanced SERS Activity of Sensor Particles. Polymer composite particles have to meet two essential requirements for address the enhanced sensing purpose. At first, particles should possess sufficient high porosity in order to provide larger available area for analytes interaction. And second, the particles have to carry high density of Ag nanoparticles at the surface for adsorption of analyte molecules and for the optimized surface-enhanced Raman scattering (SERS) sensing. The water content in the microfluidically formed droplets is responsible for the formation of a gel-like state[48] of the obtained particles and is dependent on their swellability. The porous structure of polymer matrix becomes visible after drying. SEM images of the particle surface indicate nanopores with a diameter in the order of magnitude of about 200 nm and below (Figure 3a). It is assumed that additional much smaller pores are also present in the polymer matrix. As the amount of the cross-linking agent (bisacylamide) increases in the monomer mixture, the matrix becomes harder, and the porosity decreases subsequently (Figure 3b).

The UV source induces the photochemical activation for in situ formation of Ag nanoparticles in the polymer matrix. In a triplet state, photoinitiator is known to undergo α-cleavage and generates a pair of radicals[49] as shown in Scheme 1. The

Scheme 1. Scheme for the Photochemical Synthesis of Polymer Composites Microparticles Where Photopolymerization and Photoreduction Takes Place Simultaneously

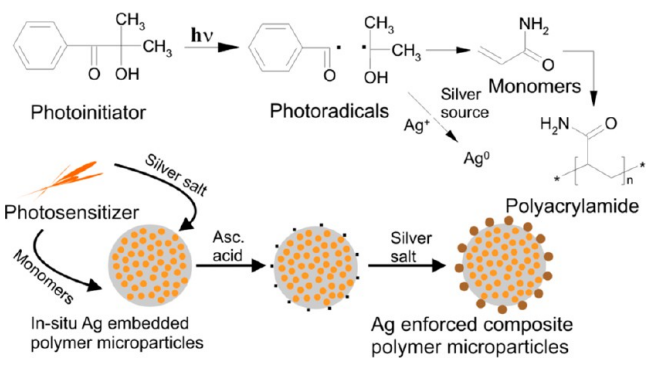

DOI: 10.1021/acsami.5b00604
ACS Appl. Mater. Interfaces 2015, 7, 10742−10754

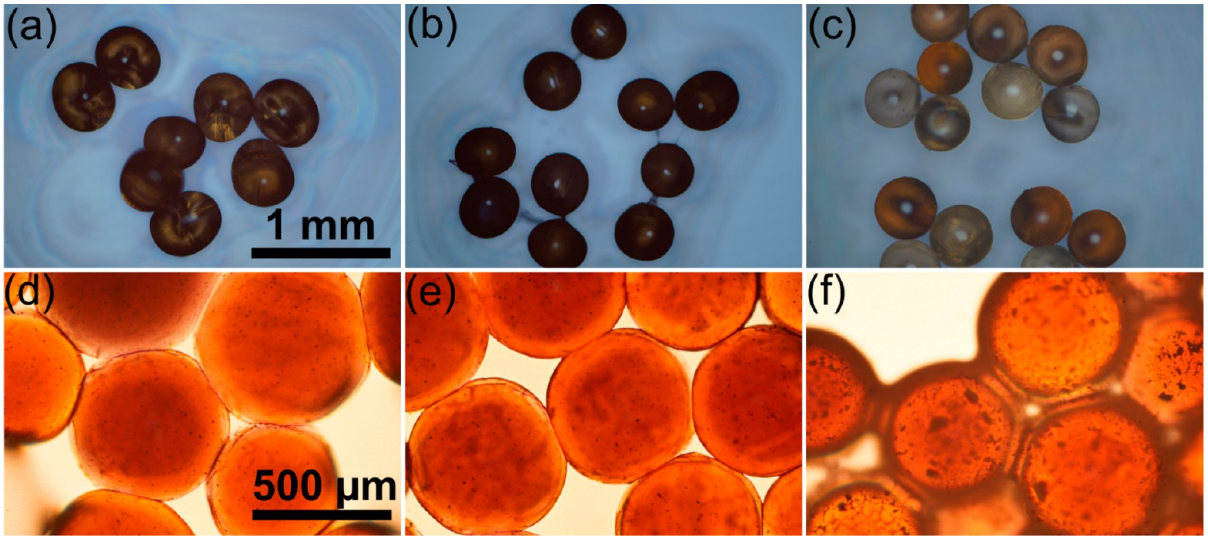

Figure 4. (a–c) Light microscope images of the polyacrylamide microparticles with different amount of embedded silver (images taken by incident light from the top of microscope): (a) 40 mM, (b) 80 mM, and (c) mixture of microparticles with different amounts of embedded silver (0, 10, 20, and 30 mM), (d–f) optical images by transmission light of 60 mM Ag embedded Ag enforced polyacrylamide particles with different concentration of enforced Ag amount on the surface of polymer particles: (d) 2.5, (e) 5, and (f) 10 mM. Scale bar for image a–c is 1 mm, and for image d–f is 500 μm.

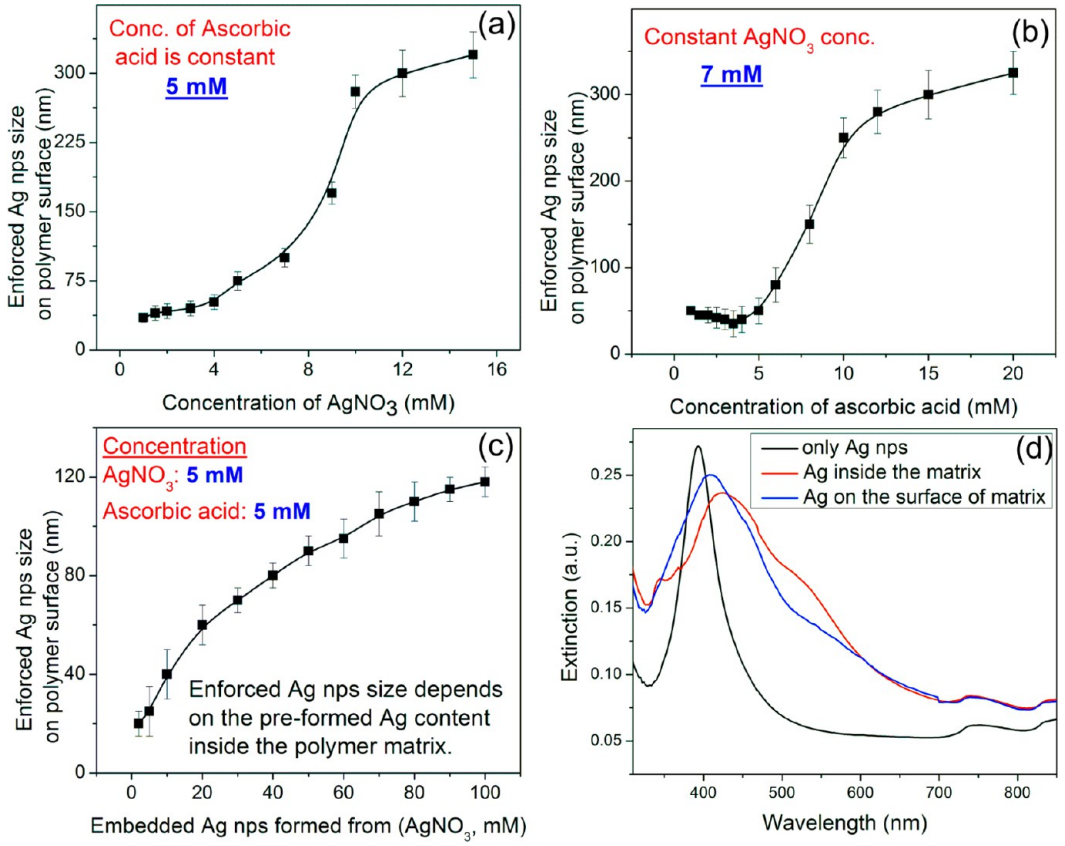

Figure 5. Graphical results of the dependence of Ag nanoparticles average sizes at the surface of matrix on different reaction conditions: (a) at different concentration of silver salt, (b) at different concentration ascorbic acid, and (c) at the different concentration of $AgNO_3$ in the matrix during in situ synthesis, and (d) UV–visible spectra of the polyacrylamide/silver composites microparticles of only colloidal Ag nanoparticles (black line), 40 μm sized polymer matrix with 60 mM embedded Ag (in situ formation of Ag nanoparticles when 60 mM $AgNO_3$ was used) (red line), and 40 μm sized polymer matrix with 5 mM enforced Ag nanoparticles (blue line).

radicals quickly supply the electrons and reduce Ag^+ ions to form Ag^0 and Ag nanoparticles, and initiate at the same time the polymerization of the acrylamide monomers. The homogeneous distribution of the formed Ag nanoparticles is a result of fine distribution of silver salt together with the monomer phase. The effect of different concentrations of Ag in

DOI: 10.1021/acsami.5b00604
ACS Appl. Mater. Interfaces 2015, 7, 10742–10754

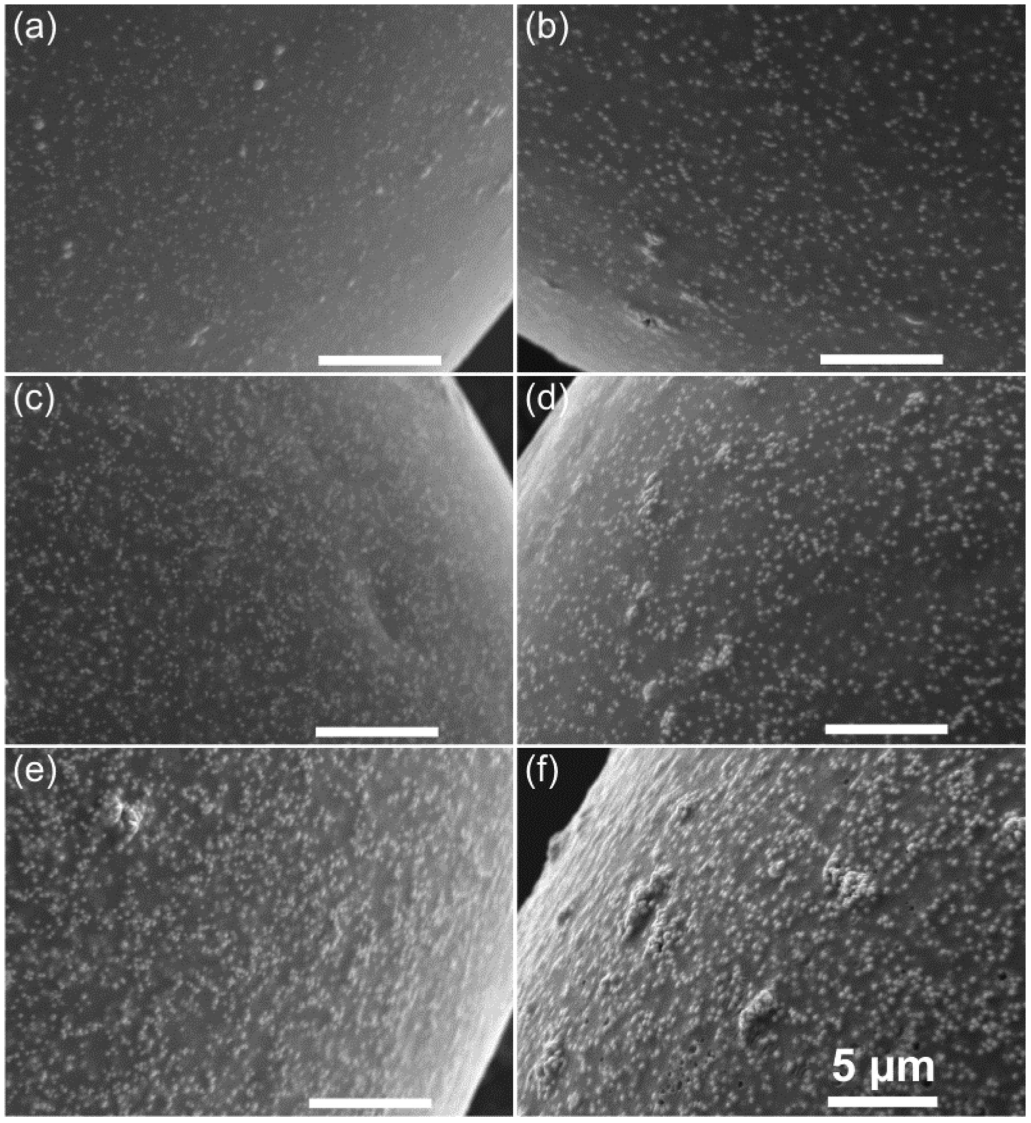

Figure 6. SEM images of the polymer composite particles for comparison of the different sizes of enforced (deposited) Ag nanoparticles on the Ag embedded polyacrylamide microparticles via Ag catalyzed Ag nanoparticles synthesis: (a) 2.5 mM ascorbic acid and 2 mM $AgNO_3$, (b) 5 mM ascorbic acid and 1.5 mM $AgNO_3$; (c) 5 mM ascorbic acid and 2 mM $AgNO_3$, (d) 10 mM ascorbic acid and 1.5 mM $AgNO_3$; (e) 5 mM ascorbic acid and 5 mM $AgNO_3$; and (f) 10 mM ascorbic acid and 5 mM $AgNO_3$.

the polymer matrix has been investigated here; the higher the salt concentration, the more and larger Ag nanoparticles were obtained, which can be concluded from the obtained colors of the sensor particles (Figure S7 in the Supporting Information). Figure 4a−c represents the optical images of the Ag embedded particles (images taken by applying incident light from the top of microscope). Generated particles with higher amount of embedded Ag nanoparticles (80 mM) are dark brown in color (Figure 4b) compared to the light brown colored particles of lower Ag loading (40 mM, Figure 4a). Moreover, the colorless sensor particles are also visualized in Figure 4c (together with different Ag-loaded particles) which are obtained without Ag nanoparticles formation. Several of Ag atoms combined and forms the smaller Ag cluster, and even without capping agent and further growth, the particles are stable against agglomeration because they are well fixed in the semisolid gel-like state of the polymer matrix. The embedded Ag acts as nuclei for further deposition of Ag on the surface, because SERS sensing activity of the primarily formed particles can only be enhanced by higher density of Ag at surface. Therefore, for further Ag enhancement, 50 μL of an aqueous solution of ascorbic acid (5 mM) was injected into 20 μL of particle suspension containing about 10 particles. Fifty microliters of $AgNO_3$ (in the range between 2.5 mM and 10 mM depending on the intended degree of Ag enforcement) have been added in small portions (about 50 μL) under vigorous stirring to this mixture. Even in the absence of polymer particles, only a slow redox reaction between the ascorbic acid and Ag^+ ions takes place; a fast formation of metallic Ag is observed in the presence of the polymer particles containing photochemically preformed Ag nanoparticles. Such Ag-catalyzed Ag deposition turns out to be visible immediately at the addition point of $AgNO_3$ solution by an intensification of the yellow color of the polymer particles. Further deepening into a brown and then more and more black-colored composite particles obtained with further addition of Ag^+ ions. The color change is realized due to the growth of Ag nanoparticles inside the polymer matrix through pores and at the surface. A typical situation of the polymer

DOI: 10.1021/acsami.5b00604
ACS Appl. Mater. Interfaces 2015, 7, 10742−10754

particles surface after the enforcement of homogeneous Ag nanoparticles is shown in Figure 3c. The formation and tuned deposition of Ag at different concentration can easily be visualized by light microscopy characterization (Figure 4d–f). Additionally, further variation of Ag nanoparticles (size up to 250 nm diameters) on surface can be uniformly tuned by altering the concentration ratios of $AgNO_3$ and ascorbic acid. Enforced Ag nanoparticles are adsorbs on the surface of matrix once it formed. When a lower concentration of ascorbic acid (2.5 mM) was used, the formed Ag nanoparticles are about 40 and 65 nm at 2 mM and 5 mM $AgNO_3$ concentration, respectively. When the concentration of the ascorbic acid was increased gradually at the initial range, the smaller-sized Ag nanoparticles were obtained in higher numbers at similar $AgNO_3$ concentration. However, further increase in ascorbic acid concentration enhances the size of generated Ag nanoparticles on surface, and it can be expected that it is a result of spontaneous aggregation via growth on preformed Ag nanoparticles. In addition, the formation of larger Ag nanoparticles turns out at higher $AgNO_3$ concentration. Therefore, about 110 nm sized Ag nanoparticles on the microgel particles surface are formed at 5 mM ascorbic acid and 7 mM $AgNO_3$ solution. Figures 5 and 6 display the results for size-tuned Ag nanoparticles and their densities on the surface of microgel particles.

A plasmonic character of the sensor particles is well reflected by the optical spectra of particles suspension (Figure 5d). It is well-known that the collective oscillation of the conduction electron takes place at the surface of Ag nanoparticles upon irradiation of electromagnetic waves (light) which generally referred to as localized surface plasmon resonance (LSPR).[50] Here, for the colloidal suspension of pure Ag nanoparticles, it is marked by the characteristic strong absorption near about 400 nm of Ag nanoparticles. In contrast to the sharp plasmon absorption peak of a pure colloidal solution of smaller Ag nanoparticles,[51] the peak become significantly broadened in the case when Ag nanoparticles are embedded in a microgel interior. In addition, the absorption peak of composite microgel particles shifts to the higher wavelength. As shown in Figure 5d, the absorption peak moved to about 425 nm when Ag nanoparticles were distributed (during in situ synthesis) inside the polymer matrix. Broadening and bathochromic shift of a fundamental plasmon peak is also enhanced with increasing silver deposition amount (aggregation size) on the surface of Ag-embedded microgel particles (Figure 5d and Scheme 2). It is proven that the plasmon peak becomes broadened and red-shifted with increase in the size of Ag nanoparticles.[52] On other side, the broadness of a peak is also depends on the size of Ag loaded polymer matrix. A comparatively sharp absorption peak is realized when Ag-embedded polymer particles are of smaller size. With similar concentration of Ag nanoparticles inside the polymer matrix, the peak becomes comparatively broader for 150 μm sized polymer particles (Figure S13 in the Supporting Information). A higher loading of Ag nanoparticles in the micrometer sized polymer matrix makes them settled down quickly in the aqueous solution. Therefore, the measurements of the optical spectra of bigger sized sensor particles were difficult. Usually in anisotropic Ag nanoparticles, the SPR band is often divided into two different modes, a transverse mode and a longitudinal mode.[50] Here, the formation of larger Ag nanoparticles takes place in the case of higher $AgNO_3$ precursor solution, which also gives two different peaks similar to the anisotropic nanoparticles. A detail study for the different shape-

Scheme 2. Schematic Representation for the Tuning of Size of Polymer Particles, Ag Nanoparticles inside and outside of the Matrix, Porosity, and the Impact of Tuned Composite Particles on Signal Intensity of SERS and Plasmonic Spectra

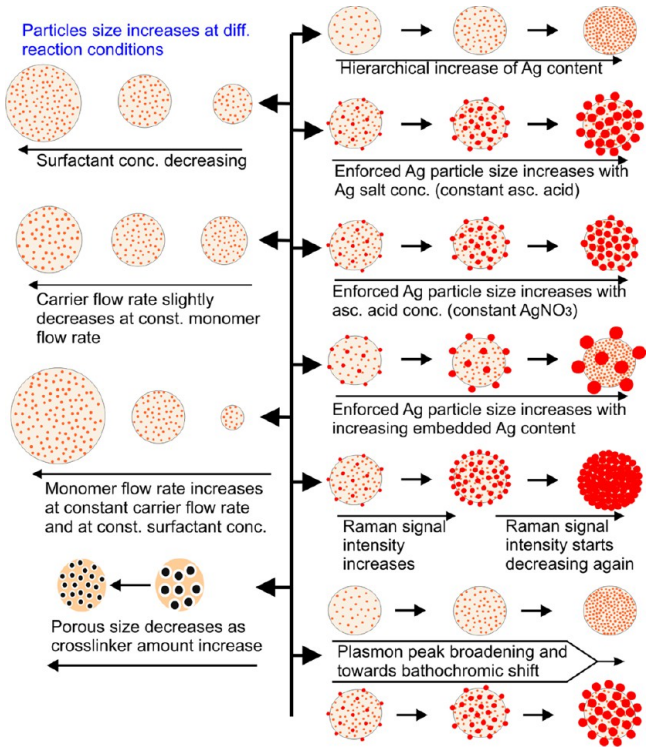

forming mechanisms of Ag nanoparticles is beyond the scope of this article. However, for comparison, UV/vis spectra of the different composite particles have been measured here (Figures S11–S13 in the Supporting Information), and a detailed study for the SERS sensing of composite microparticles with various biochemical molecules are presented.

3.4. Surface-Enhanced Raman Scattering (SERS) Sensing Applications. Raman spectroscopy is an important tool for detecting and identifying the molecules in correspondence to their unique energy level of vibrations and Raman fingerprints.[29] When the analyte molecules are adsorbed on the surface of metal nanoparticles and metal nanoparticles are immobilized to a solid support, the local electromagnetic field around the nanoparticles can enhance the Raman scattering outcome.[53] An intense local electric field within a few nanometers at the surface of adsorbed Ag nanoparticles can be generated by LSPR. Such near-field effect can advance Raman scattering cross-section of molecules adsorbed onto the surface of Ag nanoparticles. This phenomenon of enhancing the Raman scattering is called surface-enhanced Raman scattering (SERS).[54] It is well-known that the SERS intensity depends crucially on the wavelength and strength of the plasmon propagating at the surface of nanostructure.[55] The SERS enhancement factor, i.e., the ratio between Raman signals from the applied number of molecules in the presence and in the absence of the nanostructure, strongly depends on the size, shape and composition of the SERS substrate that give rise to the effect.[56] Rapid and sensitive fingerprint information on various chemical and biological species with high reproducibility can only be obtained by using reliable, stable, well-defined and uniform SERS substrate.[55] In past decade, a large number of SERS substrates have been developed for such purpose with

DOI: 10.1021/acsami.5b00604
ACS Appl. Mater. Interfaces 2015, 7, 10742–10754

unique chemical compositions.[56−59] In our work, the synthesized sensor particles possess enhanced Ag surface for providing plenty of "hot spots" for the uniform SERS outcome and also provide long-term stability, and therefore, can be used as a powerful particles-based SERS substrate. SERS test measurements have been carried out in a compact arrangement by using different size and composition tuned sensor particles. Approximately 10 sensor particles of 80 μm size without Ag enforcement were applied under the focus of a laser beam (green laser with 532 nm excitation laser source) where no any Raman signals has been obtained. In contrast, higher signals intensity arises if Ag nanoparticles were deposited on the surface significantly (Figure 7a−-f). The appearing peaks correspond to vibration resonances of the polymer matrix. The signal intensities increase with increasing amount of Ag enhancement up to an applied concentration of 150 mM $AgNO_3$ in the enforcement procedure. Further $AgNO_3$ concentrations causes the deposition of very dense Ag aggregates (Figure 7e) on the particles surface and hence the SERS signal intensity decreased drastically because the random and intense aggregation of Ag nanoparticles cover the entire surface of polymer matrix and fill the nanogaps between adjacent Ag nanoparticles from where huge enhanced effect might originated (hot spots).[56,59] Sensor particles with lower Ag enhancement (30 mM) yields lower signal intensity compare to the particles of higher Ag enhancement (100 mM).

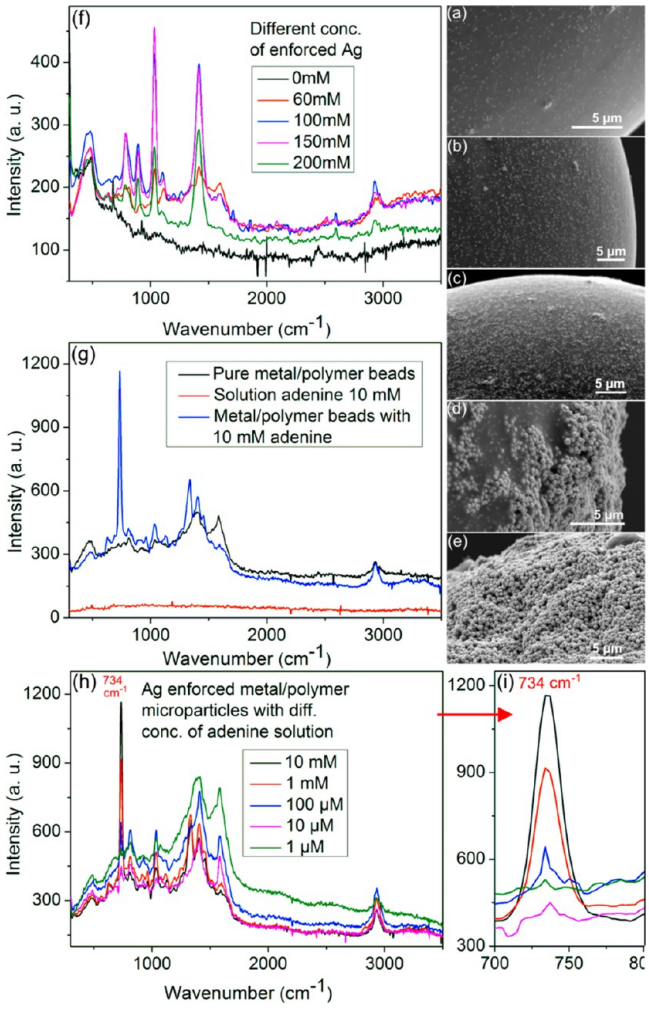

Figure 7. SEM images of the silver/polymer composite microparticles with different amount of silver on the surface: (a) 2, (b) 5, (c) 20, (d) 80, and (e) 160 mM. SERS spectra of the composite microparticles after interaction with different concentration of analytes: (f) tuning of the SERS signal intensity by applying different concentration of silver enforcements on the surface of polymer composite microparticles, SERS intensity consistently increases with increase in silver amount, but decreased down again when surface is completely covered with silver; (g) test SERS measurements of polyacrylamide microparticles after interaction with 10 mM adenine (analyte); and (h) tuned SERS spectra of microparticles after interaction with different concentrations of adenine. (i) Magnified image of peak position of graph h. SERS intensity consistently increases with increasing adenine concentration on Ag enforced polyacrylamide composite microparticles.

SERS sensing effect depends on the applied concentration of analyte molecules together with Ag deposition amount on the surface. A biochemical molecule adenine, for instance, has been monitored for proving the sensing platform of the produced sensor particles in a compact SERS arrangement. The SERS effect of the sensor particles (polyacrylamide/silver composite particles) is well reflected by the comparison of three spectra (Figure 7g). Pure adenine solution as well as only sensor particles (without analyte interaction) does not show any significant fingerprint information. The feature of the fingerprint information observed when adenine solution interact with composite particles by advancing Raman scattering cross-section of molecules adsorbed onto the surface of Ag nanoparticles. The broad band peaks between about 1450 and 1650 cm^{-1} can be obtained due to the interaction of Ag nanoparticles with polyacrylamide matrix. An intense and sharp SERS signal observed at 738 cm^{-1} when adenine solution applied to the Ag enforced porous polymer matrix. A strong Raman peak at 738 cm^{-1} features the ring breathing effect, and another strong peak at 1330 cm^{-1} is obtained because of the ring stretching effect. Adenine molecules are adsorbs on the surface of composite matrix and penetrate inside within a few nanometer of its surface. During such an event with irradiation of light, the local electromagnetic field around the particles surface enhance the Raman light by millions of factor.[29] This resulted in strong enhancements of SERS signal which is observed at 738 cm^{-1} (Figure 7g). Moreover, the enhancement of SERS signals is strongly dependent on adenine concentration. Even during the lower concentration of adenine (1 μM), the SERS signal of the sensor particles certainly obtained at 738 cm^{-1} due to the ring breathing effect, but with very low intensity. The SERS intensity consistently increases with increasing adenine concentration up to 1 mM and 10 mM (Figure 7h).

SERS biosensing is a highly sensitive and selective technique for use in the detection of wide range of biological samples and disease.[60] Raman microscopy provides specific information about vibrational energy levels of chemical bonds of the molecules. For molecules to exhibit the Raman scattering must have polarizability[61] where deformation of the electron configuration takes place, and shows the characteristic SERS sensing effect (hierarchical) after interaction with particles surface. L-Lactic acid, for instance, makes interaction with Ag surface and showing Raman fingerprint information with the intense spectral peaks at about 860 and 1410 cm^{-1} which can be obtained due to the Ag−OH and Ag−O bond of carboxylic acid group of L-lactic acid and also could be due to the substrate (sensor particles with 40 mM embedded Ag) as shown in Figure 8a−c. It is also assumed that 860 cm^{-1} band can be obtained from the C−CO stretching of L-lactic acid.[62] The

DOI: 10.1021/acsami.5b00604
ACS Appl. Mater. Interfaces 2015, 7, 10742−10754

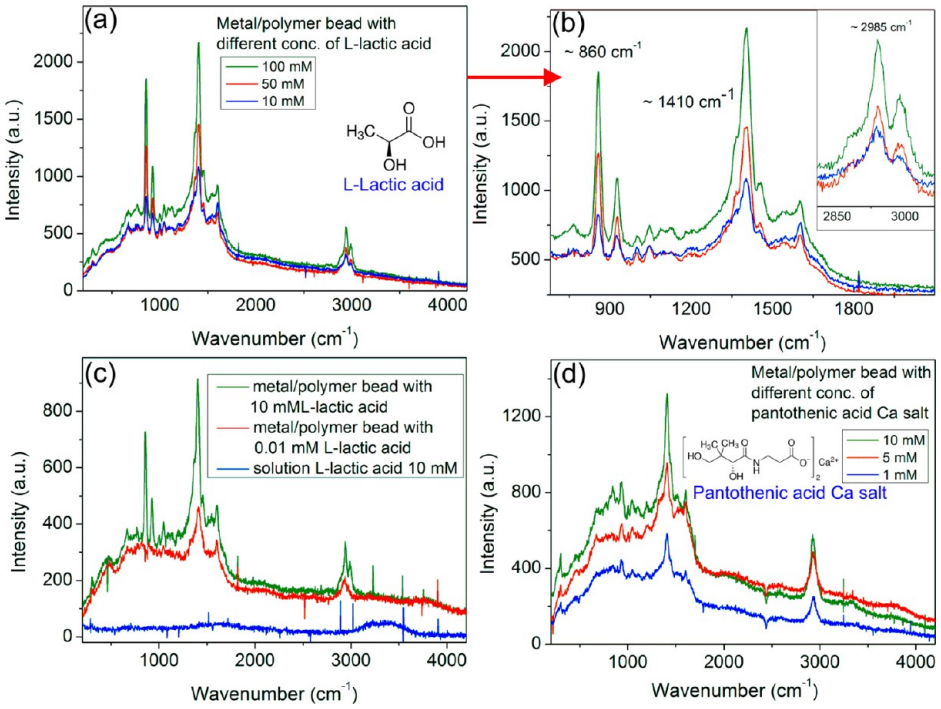

Figure 8. SERS spectra of the silver/polymer composite sensor microparticles after interaction with different concentrations of different analytes: (a, b) Normal and magnified SERS spectra with tuned SERS signals after interaction with different concentrations of L-lactic acid (analyte) on the Ag enforced polyacrylamide microparticles. (c) Controlled measurement and comparison of SERS signal position with average and very low concentration of L-lactic acid analyte on microparticles. (d) Tuned SERS spectra of composite microparticles after interaction with different concentrations of pantothenic acid analyte. The sensor particles with 60 mM embedded Ag and 40 mM enforced Ag was used for all measurements in this figure.

SERS measurement of only polymer matrix (without enforced Ag) even after the interaction with higher concentration of L-lactic acid (10 mM) gives no any significant peak or band (it shows like horizontal line similar to the spectrum of free L-lactic acid solution shown in Figure 8c, blue line). Moreover, only free L-lactic acid solution also not showing any fingerprint information. Thus, it can be concluded that the enhancement of both significant peaks can obtained only after the interaction of L-lactic acid with Ag surface of the sensor particles which is supported by the fact that the used sensor particles can be used as a versatile SERS substrate for the particles-based sensing application of biomolecules. L-Lactic acid is a simple and effective indicator for estimating physiological function, and one of the significant metabolites in blood.[62−64] The severe rise in the L-lactic acid concentration cause several clinical symptoms such as congestive heart failure.[64] And therefore, SERS platform provides the easy identification of L-lactic acid information upon utilization of a reliable SERS substrate. The used sensor particles in our study provide significant fingerprint information on L-lactic acid down to the lowest concentration of 10 μm even at lower excitation source (532 nm). Such similar kinds of many analytes can easily be detected via SERS platform by using microfluidically prepared sensor particles as a SERS substrate. Obtained sensor particles can also be applicable for the detection of vitamins and amino acids by using compact SERS arrangement. Pantothenic acid is a water-soluble vitamin and also an essential nutrient for many animals. The interaction of 1 mM pantothenic acid (Ca salt) with Ag/polyacrylamide sensor particles produces significant fingerprint information. The SERS band between 1300 and 1650 cm^{-1} can be obtained after the interaction of Ag with polyacrylamide surface in the presence of pantothenic acid, and the moderate peaks between 700 and 900 cm^{-1} appeared might be due to the Ag−O bond vibrations (Figure 8d). The SERS signal intensities consistently increases with applied concentrations of pantothenic acid. Similarly, in case of an amino acid (histidine), the tuned SERS sensing can easily detectable by obtained sensor particles. Free histidine solution does not produce any Raman signature whereas the intense SERS sensing signals appeared after the interaction of histidine molecules with the surface of sensor particles (Figure S14 in the Supporting Information). The SERS signal at about 730 cm^{-1} is the result of ring breathing effect.

Silver is more attractive for optoelectronic and sensing because of its higher plasmonic efficiency and superior electromagnetic enhancement in the visible range.[65] Usually, the surfactant or polymer as capping agents are required for the stability against undesired aggregation in a solution based silver nanoparticles synthesis. Such adsorbed surface layers of molecules restrict the application of silver material in biosensing or SERS because they prevent the adsorption of the reporter molecules on the nanoparticles surface with the identification of compounds of interest.[65] It is important to note that no any additional stabilizer was required here upon the growth of Ag nanoparticles as embedded Ag acts as nuclei which allow further Ag enforcement in a regular manner at precise reaction condition. Therefore, the Ag surface is suitable for the interaction of the analytes of interest. It should also be mentioned that the SERS intensity with respect to the excitation wavelength is not comparable as the powers of the lasers are different. Particularly here we have used only one laser power source (532 nm), and compared the SERS results with different concentrations and types of analytes as well as differently composed sensor particles. Overall, the composition

DOI: 10.1021/acsami.5b00604
ACS Appl. Mater. Interfaces 2015, 7, 10742−10754

tuned Ag/polyacrylamide sensor particles can be used as a powerful particle-based SERS substrate for identification of biomolecules and organic compounds in a batch as well as in a continuous flow condition.

4. CONCLUSIONS

The investigation shows that polymer/silver composite sensor particles of cross-linked polyacrylamide with precisely tuned diameters between about 30 and 600 μm have been reproducibly prepared by the application of a micro cross-flow arrangement via droplet generation for a suspension polymerization. The droplets, which are released from a micro holeplate and transported through a micro tube, are polymerized by photochemical initiation in analogy to the procedure known from micro coflow and flow-focusing arrangements. Channel diameter and flow rate ratio for shear force control the size of generated droplet. Beside these factors, the role of concentration of surfactant was found to be dominating for tuning the polymer particles size in broad size spectrum with homogeneous character. Together with particles size, the porosity on the polymer matrix can also be tuned which is very crucial for stronger SERS sensing application. The required high content of distributed metallic silver inside the polymer matrix is achieved by a combination of in situ formation of small metal nanoparticles during the flow process and a silver-catalyzed silver deposition in a subsequent batch process for SERS-active sensor particles. The sizes of finally obtained silver nanoparticles were regularly tuned between 40 and 250 nm by the variation in concentrations of reducing agents and silver ions during the enforcement process. SERS measurements with different analytes show a strong enhancement of Raman signal with increasing silver content of the composite particles. These complex composite particles can be used for SERS sensing when different biomolecules and analyte molecules are adsorb on the surface via chemical reaction in a droplet-based microfluidic arrangement as well as in the batch process. Overall, microfluidically prepared size and composition tuned Ag/polyacrylamide sensor particles can be used as a powerful particle-based SERS substrate for identification of different biomolecules and organic compounds.

■ ASSOCIATED CONTENT

Supporting Information

Scheme, tabular results of polyacrylamide particles size, SEM images of all size variation at different microfluidic reaction condition, SEM images of Ag enforcement at very low and very high concentration, additional UV/vis spectra for larger-sized polymer/silver composite particles, additional SERS measurements, camera pictures of the microreactor. The Supporting Information is available free of charge on the ACS Publications website at DOI: 10.1021/acsami.5b00604.

■ AUTHOR INFORMATION

Corresponding Author

*E-mail: nikunjkumar.visaveliya@tu-ilmenau.de. Fax: +49 3677 69 3173. Tel: +49 3677 69 3655.

Notes

The authors declare no competing financial interest.

■ ACKNOWLEDGMENTS

We thank Steffen Schneider and Dr. Alexander Groß for their experimental assistant. The support for the investigations by BMBF (project Bactocat, Kz 031A161A) is gratefully acknowledged.

■ REFERENCES

(1) Visaveliya, N.; Li, S. N.; Köhler, J. M. Heterogeneous Nanoassembling: Microfluidically Prepared Poly(Methyl Methacrylate) Nanoparticles on Ag Microrods and Zno Microflowers. *Part. Part. Syst. Charact.* **2013**, *30*, 614−623.

(2) Sun, W.; Hayden, S.; Jin, Y. H.; Rong, Y.; Yu, J. B.; Ye, F. M.; Chan, Y. H.; Zeigler, M.; Wu, C. F.; Chiu, D. T. A Versatile Method for Generating Semiconducting Polymer Dot Nanocomposites. *Nanoscale* **2012**, *4*, 7246−7249.

(3) Balazs, A. C.; Emrick, T.; Russell, T. P. Nanoparticle Polymer Composites: Where Two Small Worlds Meet. *Science* **2006**, *314*, 1107−1110.

(4) Park, J. I.; Saffari, A.; Kumar, S.; Gunther, A.; Kumacheva, E. Microfluidic Synthesis of Polymer and Inorganic Particulate Materials. *Annu. Rev. Mater. Res.* **2010**, *40*, 415−443.

(5) Tao, A. R.; Habas, S.; Yang, P. Shape Control of Colloidal Metal Nanocrystals. *Small* **2008**, *4*, 310−325.

(6) Visaveliya, N.; Kohler, J. M. A Self-Seeding Synthesis of Ag Microrods of Tuned Aspect Ratio: Ascorbic Acid Plays a Key Role. *Nanotechnology* **2013**, *24*, 345604.

(7) Koehler, J. M.; Moeller, F.; Schneider, S.; Guenther, P. M.; Albrecht, A.; Gross, G. A. Size-Tuning of Monodisperse PMMA Nanoparticles by Micro-Continuous-Flow Polymerization Using a Silicon Micro-Nozzle Array. *Chem. Eng. J.* **2011**, *167*, 688−693.

(8) Haeberle, S.; Zengerle, R. Microfluidic Platforms for Lab-on-a-Chip Applications. *Lab Chip* **2007**, *7*, 1094−1110.

(9) Edel, J. B.; Fortt, R.; deMello, J. C.; deMello, A. J. Microfluidic Routes to the Controlled Production of Nanoparticles. *Chem. Commun.* **2002**, 1136−1137.

(10) Marre, S.; Jensen, K. F. Synthesis of Micro and Nanostructures in Microfluidic Systems. *Chem. Soc. Rev.* **2010**, *39*, 1183−1202.

(11) Theberge, A. B.; Courtois, F.; Schaerli, Y.; Fischlechner, M.; Abell, C.; Hollfelder, F.; Huck, W. T. S. Microdroplets in Microfluidics: An Evolving Platform for Discoveries in Chemistry and Biology. *Angew. Chem., Int. Ed.* **2010**, *49*, 5846−5868.

(12) Zang, E.; Brandes, S.; Tovar, M.; Martin, K.; Mech, F.; Horbert, P.; Henkel, T.; Figge, M. T.; Roth, M. Real-Time Image Processing for Label-Free Enrichment of Actinobacteria Cultivated in Picolitre Droplets. *Lab Chip* **2013**, *13*, 3707−3713.

(13) Teh, S. Y.; Lin, R.; Hung, L. H.; Lee, A. P. Droplet Microfluidics. *Lab Chip* **2008**, *8*, 198−220.

(14) Anton, N.; Bally, F.; Serra, C. A.; Ali, A.; Arntz, Y.; Mely, Y.; Zhao, M. J.; Marchioni, E.; Jakhmola, A.; Vandamme, T. F. A New Microfluidic Setup for Precise Control of the Polymer Nanoprecipitation Process and Lipophilic Drug Encapsulation. *Soft Matter* **2012**, *8*, 10628−10635.

(15) Knauer, A.; Schneider, S.; M?ller, F.; Csaki, A.; Fritzsche, W.; Köhler, J. M. Screening of Plasmonic Properties of Composed Metal Nanoparticles by Combinatorial Synthesis in Micro-Fluid Segment Sequences. *Chem. Eng. J.* **2013**, *227*, 80−89.

(16) Chang, Z. Q.; Serra, C. A.; Bouquey, M.; Kraus, I.; Li, S. N.; Köhler, J. M. Multiscale Materials from Microcontinuous-Flow Synthesis: Zno and Au Nanoparticle-Filled Uniform and Homogeneous Polymer Microbeads. *Nanotechnology* **2010**, *21*, 015605.

(17) Gai, S. L.; Yang, P. P.; Li, C. X.; Wang, W. X.; Dai, Y. L.; Niu, N.; Lin, J. Synthesis of Magnetic, up-Conversion Luminescent, and Mesoporous Core-Shell-Structured Nanocomposites as Drug Carriers. *Adv. Funct. Mater.* **2010**, *20*, 1166−1172.

(18) Liz-Marzan, L. M.; Philipse, A. P. Synthesis and Optical Properties of Gold-Labeled Silica Particles. *J. Colloid Interface Sci.* **1995**, *176*, 459−466.

(19) Lin, Y.-S.; Wu, S.-H.; Hung, Y.; Chou, Y.-H.; Chang, C.; Lin, M.-L.; Tsai, C.-P.; Mou, C.-Y. Multifunctional Composite Nanoparticles: Magnetic, Luminescent, and Mesoporous. *Chem. Mater.* **2006**, *18*, 5170−5172.

DOI: 10.1021/acsami.5b00604
ACS Appl. Mater. Interfaces 2015, 7, 10742−10754

(20) Chang, Z. Q.; Serra, C. A.; Bouquey, M.; Prat, L.; Hadziioannou, G. Co-Axial Capillaries Microfluidic Device for Synthesizing Size- and Morphology-Controlled Polymer Core-Polymer Shell Particles. *Lab Chip* **2009**, *9*, 3007−3011.
(21) Koher, J. M.; Marz, A.; Popp, J.; Knauer, A.; Kraus, I.; Faerber, J.; Serra, C. Polyacrylamid/Silver Composite Particles Produced Via Microfluidic Photopolymerization for Single Particle-Based Sers Microsensorics. *Anal. Chem.* **2013**, *85*, 313−318.
(22) Köhler, J. M.; Kraus, I.; Faerber, J.; Serra, C. Continuous-Flow Preparation of Nanoporous Metal/Polymer Composite Particles by in Situ Synthesis of Silver Nanoparticles in Photopolymerized Acrylate/Diethylene Glycol Droplets. *J. Mater. Sci.* **2013**, *48*, 2158−2166.
(23) Nie, Z. H.; Xu, S. Q.; Seo, M.; Lewis, P. C.; Kumacheva, E. Polymer Particles with Various Shapes and Morphologies Produced in Continuous Microfluidic Reactors. *J. Am. Chem. Soc.* **2005**, *127*, 8058−8063.
(24) Seo, M.; Nie, Z. H.; Xu, S. Q.; Mok, M.; Lewis, P. C.; Graham, R.; Kumacheva, E. Continuous Microfluidic Reactors for Polymer Particles. *Langmuir* **2005**, *21*, 11614−11622.
(25) Champion, J. A.; Mitragotri, S. Role of Target Geometry in Phagocytosis. *Proc. Natl. Acad. Sci. U.S.A.* **2006**, *103*, 4930−4934.
(26) Farokhzad, O. C.; Cheng, J. J.; Teply, B. A.; Sherifi, I.; Jon, S.; Kantoff, P. W.; Richie, J. P.; Langer, R. Targeted Nanoparticle-Aptamer Bioconjugates for Cancer Chemotherapy in Vivo. *Proc. Natl. Acad. Sci. U.S.A.* **2006**, *103*, 6315−6320.
(27) Bertrand, N.; Wu, J.; Xu, X. Y.; Kamaly, N.; Farokhzad, O. C. Cancer Nanotechnology: The Impact of Passive and Active Targeting in the Era of Modern Cancer Biology. *Adv. Drug Delivery Rev.* **2014**, *66*, 2−25.
(28) Peer, D.; Karp, J. M.; Hong, S.; Farokhzad, O. C.; Margalit, R.; Langer, R. Nanocarriers as an Emerging Platform for Cancer Therapy. *Nat. Nanotechnol.* **2007**, *2*, 751−760.
(29) Anker, J. N.; Hall, W. P.; Lyandres, O.; Shah, N. C.; Zhao, J.; Van Duyne, R. P. Biosensing with Plasmonic Nanosensors. *Nat. Mater.* **2008**, *7*, 442−453.
(30) Polavarapu, L.; Perez-Juste, J.; Xu, Q. H.; Liz-Marzan, L. M. Optical Sensing of Biological, Chemical and Ionic Species through Aggregation of Plasmonic Nanoparticles. *J. Mater. Chem. C* **2014**, *2*, 7460−7476.
(31) Visaveliya, N.; Kohler, J. M. Single-Step Microfluidic Synthesis of Various Nonspherical Polymer Nanoparticles Via in Situ Assembling: Dominating Role of Polyelectrolytes Molecules. *Acs Appl. Mater. Interfaces* **2014**, *6*, 11254−11264.
(32) De Geest, B. G.; Urbanski, J. P.; Thorsen, T.; Demeester, J.; De Smedt, S. C. Synthesis of Monodisperse Biodegradable Microgels in Microfluidic Devices. *Langmuir* **2005**, *21*, 10275−10279.
(33) Dendukuri, D.; Doyle, P. S. The Synthesis and Assembly of Polymeric Microparticles Using Microfluidics. *Adv. Mater.* **2009**, *21*, 4071−4086.
(34) Hwang, D. K.; Dendukuri, D.; Doyle, P. S. Microfluidic-Based Synthesis of Non-Spherical Magnetic Hydrogel Microparticles. *Lab Chip* **2008**, *8*, 1640−1647.
(35) Serra, C. A.; Chang, Z. Q. Microfluidic-Assisted Synthesis of Polymer Particles. *Chem. Eng. Technol.* **2008**, *31*, 1099−1115.
(36) Köhler, J. M.; Li, S. N.; Knauer, A. Why Is Micro Segmented Flow Particularly Promising for the Synthesis of Nanomaterials? *Chem. Eng. Technol.* **2013**, *36*, 887−899.
(37) Serra, C. A.; Chang, Z. Microfluidic-Assisted Synthesis of Polymer Particles. *Chem. Eng. Technol.* **2008**, *31*, 1099−1115.
(38) Atencia, J.; Beebe, D. J. Controlled Microfluidic Interfaces. *Nature* **2005**, *437*, 648−655.
(39) Dendukuri, D.; Tsoi, K.; Hatton, T. A.; Doyle, P. S. Controlled Synthesis of Nonspherical Microparticles Using Microfluidics. *Langmuir* **2005**, *21*, 2113−2116.
(40) Waters, S. L.; Grotberg, J. B. The Propagation of a Surfactant Laden Liquid Plug in a Capillary Tube. *Phys. Fluids* **2002**, *14*, 471−480.
(41) Cabeza, V. S.; Kuhn, S.; Kulkarni, A. A.; Jensen, K. F. Size-Controlled Flow Synthesis of Gold Nanoparticles Using a Segmented Flow Microfluidic Platform. *Langmuir* **2012**, *28*, 7007−7013.
(42) Xu, S. Q.; Nie, Z. H.; Seo, M.; Lewis, P.; Kumacheva, E.; Stone, H. A.; Garstecki, P.; Weibel, D. B.; Gitlin, I.; Whitesides, G. M. Generation of Monodisperse Particles by Using Microfluidics: Control over Size, Shape, and Composition. *Angew. Chem., Int. Ed.* **2005**, *44*, 724−728.
(43) Kraus, I.; Li, S.; Knauer, A.; Schmutz, M.; Faerber, J.; Serra, C. A.; Köhler, M. Continuous-Microflow Synthesis and Morphological Characterization of Multiscale Composite Materials Based on Polymer Microparticles and Inorganic Nanoparticles. *J. Flow Chem.* **2014**, *4*, 72−78.
(44) Kelly, K. L.; Coronado, E.; Zhao, L. L.; Schatz, G. C. The Optical Properties of Metal Nanoparticles: The Influence of Size, Shape, and Dielectric Environment. *J. Phys.Chem. B* **2003**, *107*, 668−677.
(45) Li, M.; Schnablegger, H.; Mann, S. Coupled Synthesis and Self-Assembly of Nanoparticles to Give Structures with Controlled Organization. *Nature* **1999**, *402*, 393−395.
(46) Hirakawa, T.; Kamat, P. V. Charge Separation and Catalytic Activity of Ag@Tio2 Core-Shell Composite Clusters under UV-Irradiation. *J. Am. Chem. Soc.* **2005**, *127*, 3928−3934.
(47) Serra, C. A.; Khan, I. U.; Chang, Z. Q.; Bouquey, M.; Muller, R.; Kraus, I.; Schmutz, M.; Vandamme, T.; Anton, N.; Ohm, C.; Zentel, R.; Knauer, A.; Köhler, M. Engineering Polymer Microparticles by Droplet Microfluidics. *J. Flow Chem.* **2013**, *3*, 66−75.
(48) Peppas, N. A.; Hilt, J. Z.; Khademhosseini, A.; Langer, R. Hydrogels in Biology and Medicine: From Molecular Principles to Bionanotechnology. *Adv. Mater.* **2006**, *18*, 1345−1360.
(49) McGilvray, K. L.; Decan, M. R.; Wang, D. S.; Scaiano, J. C. Facile Photochemical Synthesis of Unprotected Aqueous Gold Nanoparticles. *J. Am. Chem. Soc.* **2006**, *128*, 15980−15981.
(50) Lu, X. M.; Rycenga, M.; Skrabalak, S. E.; Wiley, B.; Xia, Y. N. Chemical synthesis of novel plasmonic nanoparticles. *Annu. Rev. Phys. Chem.* **2009**, *60*, 167−192.
(51) Lee, K. S.; El-Sayed, M. A. Gold and Silver Nanoparticles in Sensing and Imaging: Sensitivity of Plasmon Response to Size, Shape, and Metal Composition. *J. Phys. Chem. B* **2006**, *110*, 19220−19225.
(52) Bastus, N. G.; Merkoci, F.; Piella, J.; Puntes, V. Synthesis of Highly Monodisperse Citrate-Stabilized Silver Nanoparticles of up to 200 Nm: Kinetic Control and Catalytic Properties. *Chem. Mater.* **2014**, *26*, 2836−2846.
(53) Dieringer, J. A.; McFarland, A. D.; Shah, N. C.; Stuart, D. A.; Whitney, A. V.; Yonzon, C. R.; Young, M. A.; Zhang, X. Y.; Van Duyne, R. P. Surface Enhanced Raman Spectroscopy: New Materials, Concepts, Characterization Tools, and Applications. *Faraday Discuss.* **2006**, *132*, 9−26.
(54) McFarland, A. D.; Young, M. A.; Dieringer, J. A.; Van Duyne, R. P. Wavelength-Scanned Surface-Enhanced Raman Excitation Spectroscopy. *J. Phys. Chem. B* **2005**, *109*, 11279−11285.
(55) Cialla, D.; Marz, A.; Bohme, R.; Theil, F.; Weber, K.; Schmitt, M.; Popp, J. Surface-Enhanced Raman Spectroscopy (SERS): Progress and Trends. *Anal. Bioanal. Chem.* **2012**, *403*, 27−54.
(56) Fan, M. K.; Andrade, G. F. S.; Brolo, A. G. A Review on the Fabrication of Substrates for Surface Enhanced Raman Spectroscopy and Their Applications in Analytical Chemistry. *Anal. Chim. Acta* **2011**, *693*, 7−25.
(57) Lin, X. M.; Cui, Y.; Xu, Y. H.; Ren, B.; Tian, Z. Q. Surface-Enhanced Raman Spectroscopy: Substrate-Related Issues. *Anal. Bioanal. Chem.* **2009**, *394*, 1729−1745.
(58) Zhang, L.; Jiang, C.; Zhang, Z. Graphene Oxide Embedded Sandwich Nanostructures for Enhanced Raman Readout and Their Applications in Pesticide Monitoring. *Nanoscale* **2013**, *5*, 3773−3779.
(59) Han, Y.; Liu, S.; Liu, B.; Jiang, C.; Zhang, Z. In Situ Loading of Ag Nanocontacts onto Silica Nanospheres: A SERS Platform for Ultrasensitive Detection. *RSC Adv.* **2014**, *4*, 2776−2782.

DOI: 10.1021/acsami.5b00604
ACS Appl. Mater. Interfaces 2015, 7, 10742−10754

(60) Shafer-Peltier, K. E.; Haynes, C. L.; Glucksberg, M. R.; Van Duyne, R. P. Toward a Glucose Biosensor Based on Surface-Enhanced Raman Scattering. *J. Am. Chem. Soc.* **2003**, *125*, 588−593.
(61) Chrimes, A. F.; Khoshmanesh, K.; Stoddart, P. R.; Mitchell, A.; Kalantar-zadeh, K. Microfluidics and Raman Microscopy: Current Applications and Future Challenges. *Chem. Soc. Rev.* **2013**, *42*, 5880−5906.
(62) Cassanas, G.; Morssli, M.; Fabrègue, E.; Bardet, L. Vibrational Spectra of Lactic Acid and Lactates. *J. Raman Spectrosc.* **1991**, *22*, 409−413.
(63) Hsu, P.-H.; Chiang, H. K. Surface-Enhanced Raman Spectroscopy for Quantitative Measurement of Lactic Acid at Physiological Concentration in Human Serum. *J. Raman Spectrosc.* **2010**, *41*, 1610−1614.
(64) Shah, N. C.; Lyandres, O.; Walsh, J. T.; Glucksberg, M. R.; Van Duyne, R. P. Lactate and Sequential Lactate−Glucose Sensing Using Surface-Enhanced Raman Spectroscopy. *Anal. Chem.* **2007**, *79*, 6927−6932.
(65) Samal, A. K.; Polavarapu, L.; Rodal-Cedeira, S.; Liz-Marzán, L. M.; Pérez-Juste, J.; Pastoriza-Santos, I. Size Tunable Au@Ag Core−Shell Nanoparticles: Synthesis and Surface-Enhanced Raman Scattering Properties. *Langmuir* **2013**, *29*, 15076−15082.

DOI: 10.1021/acsami.5b00604
ACS Appl. Mater. Interfaces 2015, 7, 10742−10754